

Article

Large Signal Stabilization of Hybrid AC/DC Micro-Grids Using Nonlinear Robust Controller

Reza Pejmanfar ¹, Mahmoud Reza Haghifam ^{2,*}, Soodabeh Soleymani ¹ and Babak Tavassoli ³

¹ Department of Electrical Engineering, Science and Research Branch, Islamic Azad University, Tehran 14778-93855, Iran; rpejmanfar@srbiau.ac.ir (R.P.); s.soleymani@srbiau.ac.ir (S.S.)

² Department of Electrical and Computer Engineering, Tarbiat Modares University, Tehran 14115-111, Iran

³ Department of Electrical and Computer Engineering, K.N. Toosi University of Technology, Tehran 16317-14191, Iran; tavassoli@kntu.ac.ir

* Correspondence: haghifam@modares.ac.ir; Tel.: +98-21-82884347

Academic Editor: Chunhua Liu

Received: 13 August 2017; Accepted: 25 October 2017; Published: 1 December 2017

Abstract: This paper presents a robust nonlinear integrated controller to improve stability of hybrid AC/DC micro-grids under islanding mode. The proposed controller includes two independent controllers where each one is responsible to control one part of the system. First controller will improve the stability of input DC/DC converter. Using this controller, the voltage of DC bus is fully stabilized such that when a large disturbance occurs, its voltage will become constant without any significant dynamic. The necessity of DC bus regulation which has not been considered in previous studies, is imminent as it not only improves voltage stability of the micro-grid but also protects consumers which are directly connected to the DC bus, against voltage variations. Frequency stability of the micro-grid is provided by the second proposed controller which is applied to output DC/AC converter of the micro-grid. Adaptive method is used to make the controllers proposed in this paper, robust. Duty cycle of converters switches are adjusted such that voltage and frequency of the micro-grid are set on the desired value in minimum possible time under transient disturbances and uncertainty of the loads as well as micro-sources characteristics.

Keywords: hybrid micro-grid; robust control; adaptive control; sliding mode; stability

1. Introduction

Recently, environmental and economic issues have attracted attentions, thus the conventional structure of power systems has changed such that many distributed generation (DG) units are connected to electrical distribution networks. This issue reduces concerns but power quality is low because there is no independent controller in these structures, both local load and the utility are affected by low quality of power [1,2]. Thus, micro-grid is introduced as a new concept to resolve inherent constraints of DG systems through appropriate control and management of local DGs and loads.

For a long time, except in special cases, most distribution networks were AC and consumers had to use AC/DC converters to match with the networks. After the deployment of micro-grids, it was observed that most micro-grids are also AC. What should be noted in micro-grids is the existence of inherently DC sources like photo voltaic panels, batteries and fuel cells and a wide range of DC Loads such as household appliances and general appliances like LED lights, computers, TVs, audio and video systems, heaters, ovens, cooking wares, etc. which are all DC [3–5]. If these appliances are supplied by an AC source, not only DC/AC and AC/DC converters are required but also power factor controller should be used to provide reactive power of the converters [3,4].

If a DC micro-grid is established, the efficiency of the system can be increased significantly and costs can be reduced by creating a short path for power transmission between DC sources and DC

loads using high efficiency converters to prevent unessential DC/AC conversion. In practice, several experimental projects like low voltage DC micro-grid has been tested in Energy Systems Research Center of Italy and Laurence National Laboratories of Berkley and results show 10% energy saving compared to conventional AC systems [1].

DC micro-grid compared to AC micro-grid has other advantages like fewer converters, less loss of distribution system and a higher efficiency. Additionally, unlike grid connected AC micro-grids, where phase and frequency tracking affect controllability and reliability, DC micro-grids do not require such tracking [5].

Since DC micro-grid is more appropriate for integrating DGs, in the case of widespread micro-grid in which different sources should be integrated complementarily to affect environment positively and reduce maintenance interval, employing a single DC micro-grid is not suitable. Therefore, the need for a hybrid AC/DC micro-grid is obvious. The advantages of these are existence both AC and DC networks in terms of simple integrations of renewable resources, higher power conversion efficiency, reducing energy storage capacity and a higher reliability. For instance, China's Electricity Network Organization has created a hybrid AC/DC micro-grid in Dongfushan Island, in which different DGs and energy reservoirs are integrated. This has increased reliability and efficiency of total power source of the island [1]. In general, the advantages of a hybrid AC/DC micro-grids can be summarized as follows [1,6–9]:

- (1) Elimination of DC/AC or AC/DC/AC power converters installed on power resources. This reduces power losses significantly.
- (2) Elimination of reactive power compensators, installed in conventional AC networks. This reduces purchase and maintenance costs and decreases lines losses and power electronic equipment losses on the end users.
- (3) Since DC loads do not cause harmonic distortion directly, the power quality on AC side can be enhanced by controlling middle converters.
- (4) As problems of negative and zero sequences current caused by unbalanced loads on AC side can be resolved on DC side, these networks are able to control the asymmetric current to a desirable extent.

A hybrid AC/DC micro-grid includes three main sections: AC micro-grid, DC micro-grid and power electronic interfaces between AC side and input distributed sources. Figure 1a shows general structure of a hybrid AC/DC micro-grid connected to the utility in which DC micro-grid is connected to the AC network through a middle converter. AC sources like wind turbines and small diesel generators and AC loads like conventional lights can be connected to AC micro-grid. On the other hand, DC power resources like photo voltaic panels, fuel cells and batteries can be connected to DC micro-grid through simple DC/DC converters. Moreover, a group of AC loads that operate with variable frequency like adjustable speed induction motors is better to be connected to DC micro-grid in optimal state [7–9].

When AC micro-grid operates in island mode, control objectives include controlling frequency and voltage to increase dynamic and transient stabilities. While in island DC micro-grid, DC voltage or current should be controlled exactly so that power sharing among DC sources and DC loads is done perfectly. Finally, the simultaneous operation of AC and DC micro-grids can manage power flux between AC and DC networks correctly such that efficiency is optimized and stability is increased [9–13].

Microgrids utilization requires a proper control schemes in order to control the power sharing as well as improve the small and large signal stabilities. Many researches have been performed on the dynamic stabilizing and power sharing control in microgrids. However, a few efforts have been made on the large signal stability and power flow control among AC and DC microsources in hybrid microgrids, mainly in the autonomous mode.

A proper method for power sharing imitated from conventional droop control of the governor system of the synchronous generators is used in AC microgrids [14–17]. To create the reference

power when multi converters working together a frequency-droop characteristic is defined. Regarding to theory of droop control method the load power sharing is done based on related droop slope of each converter [15]. Same as the above droop method the DC voltage droop approach is used for power flow control of DC microgrids. In this method power flow control is done via a virtual resistor [14,18,19]. Also a supplement method by using adjacent converters is offered to increase accuracy of the power sharing and regulation of system voltage as well as reliability improvement via individual communication infrastructure [20–22]. An autonomous power sharing method in multiple converters hybrid microgrids by establishing a superimposed frequency in the dc subgrid is presented in [23].

Real-time control of hybrid microgrids including storage system and pulsed loads is presented in [24]. In this work, the authors present a universal frequency and voltage control strategy for a hybrid AC/DC microgrid be composed of a synchronous generator, solar generation simulator and bidirectional converters.

A robust H_2/H_∞ control scheme for autonomous multidistributed microsources converter based microgrids is presented in [25] which in that voltage and frequency set points of local controllers is specified by power management system as well as hierarchical droop based scheme. Also a robust H_2/H_∞ controller is established for tracking of set point and disturbance cancelation and also raising fault ride through capability and increasing performance in dynamic and transient disturbances as well as supplying nonlinear loads.

A finite time robust control strategy for regulation of voltage and frequency and control of active and reactive powers in autonomous microgrids is presented in [26] which in that the response of the controller is very fast when various inverters are operated in complex conditions. The major advantages of the proposed control scheme are being robust against unmodeled dynamics, parametric uncertainty, loads changing and large variation of work point.

Considering the discussion above, in this paper a hybrid AC/DC micro-grid is controlled such that it can provide the stability of the micro-grid when a large signal disturbance occurs like short circuit in point of common coupling (PCC) and changing operating mode from grid connected mode to islanding mode. For this purpose, an integrated controller is used to control DC and AC parts of the micro-grid as shown in Figure 1b.

According to this figure, each unregulated DC source is connected to the AC network through two cascade converters. Input converter is a Multiphase Boost Converter (MBC) which increases DC voltage amplitude of the micro source and stabilizes output DC voltage using a robust nonlinear controller when variations of the load resistance are not known. Output converter is a DC to AC voltage source converter (VSC) which tunes amplitude, frequency and phase of the output AC voltage such that not only power can be shared in steady state but also the stability of the micro-grid when large disturbances occur is guaranteed. For these purposes, a conventional droop control with a supplementary controller is proposed.

The rest of this paper is organized as follows: Section 2 which is comprised of three subsections presents MBC and input micro sources models, how the proposed nonlinear controller is designed and its stability is proved. In Section 3 which is comprised of three subsections, VSC of the AC section is modeled and the proposed controller is designed and its stability is proved. Performance of the controllers under different disturbances is simulated numerically and the results are given in Section 4. Section 5 and presents concludes and appendix of the paper.

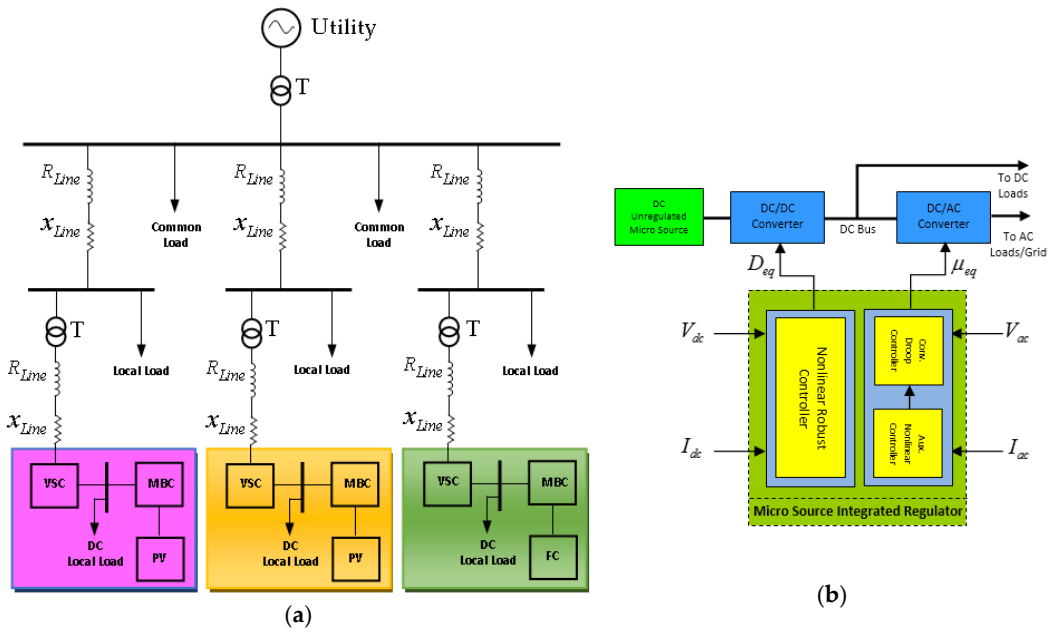


Figure 1. (a) General structure of a hybrid AC/DC micro-grid; (b) Proposed integrated controller.

2. Designing a Robust Controller to Improve Performance of the DC Section

2.1. Modeling Input DC Resources

Today, using distributed micro-sources with DC output like fuel cells and photo voltaic panels have attracted attentions due their advantages. Thus, this paper considers these micro-sources as the main power supply for micro-grids. Since the dynamics of the input micro-source affects performance of the converter and its stability, its dynamic should be considered in the general model of the system. Typical electric characteristic of fuel cells and photo voltaic panels are shown in Figure 2a,b [27,28].

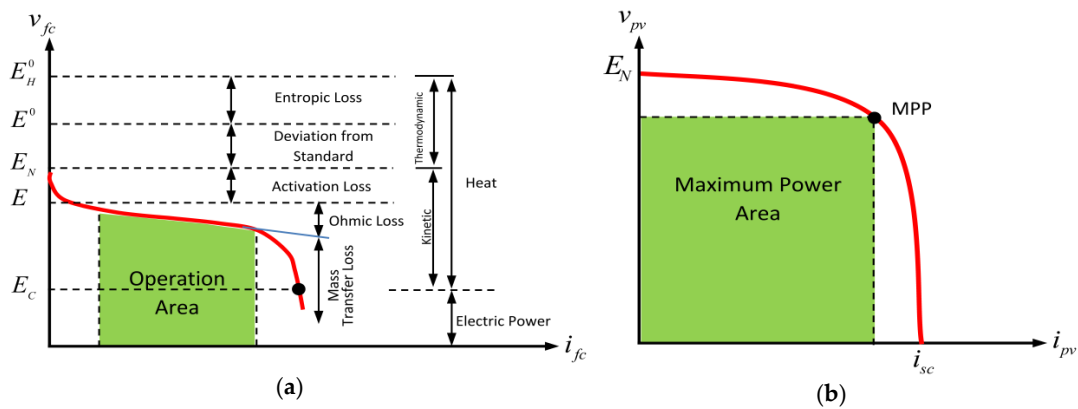


Figure 2. General electrical characteristic of micro sources (a) Characteristic of fuel cell; (b) Characteristic of photo voltaic panel.

As can be seen in Figure 2a, in a fuel cell, there is a remarkable difference between non load and full-load voltages and nonlinear dynamic in operating region is obvious. A general equation is used to represent voltage variations of the cell as follows [27]:

$$v_{fc} = E_N - A \log\left(\frac{i_{fc} - i_n}{i_0}\right) - \left[R_m(i_{fc} - i_n) + B \log\left(1 - \frac{i_{fc} - i_n}{i_{Lim}}\right)\right] \quad (1)$$

In this equation, E_N is the open circuit voltage of the cell and v_{fc}, i_{fc} are its output voltage and current (other variables are described in [14]). According to Figure 2b, electrical characteristic of the photo voltaic panels has nonlinear dynamic and it can be described as follows [28]:

$$i_{pv} = i_s - i_0 \left(\exp \left(\frac{(V_{pv} + R_s i_{pv})}{\alpha V_T} \right) - 1 \right) - \frac{V_{pv} + R_s i_{pv}}{R_{sh}} \quad (2)$$

In this equation, v_{pv}, i_{pv} are output voltage and current of panel (other variables are described in [15]). Using (1) and (2) in simulations are not appropriate, thus these equations are approximated as polynomials in the following forms:

$$v_{fc} = \sum_{k=0}^n a_k i_{fc}^k \Rightarrow v_{fc} = f(i_{fc}) \quad (3)$$

$$v_{pv} = \sum_{j=0}^m b_j i_{pv}^j \Rightarrow v_{pv} = g(i_{pv}) \quad (4)$$

2.2. Modeling Input DC/DC Converter

Conventional boost converters include an inductor (and capacitor) with a high-power switch. All DC power is converted through these two elements [12]. In these converters, not only power efficiency is low, but also high ripple in voltage and current is created. This ripple affects lifetime and efficiency of the fuel cell. Thus, here multiphase boost converters are used instead of conventional boost converters. By using these converters, generated ripple, size of inductor and power loss of switches can be decreased and reliability can be increased also the possibility to increase energy efficiency can be provided [29–38].

2.2.1. Nonlinear Model of the three phase DC/DC Boost Converter

Figure 3 shows a simple model of three phase boost converter with parallel arrangement. Inductance and series resistance of the inductors shown in Figure 3, are modeled with L_1, L_2, L_3 and r_{L1}, r_{L2}, r_{L3} . However, for simplicity it is assumed that all of the internal resistances and inductances are equal ($L_1 = L_2 = L_3 = L, r_{L1} = r_{L2} = r_{L3} = r_L$).

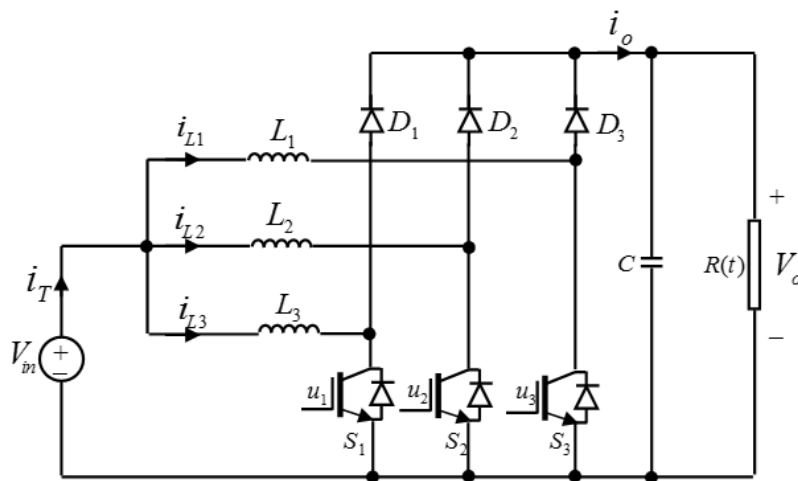


Figure 3. Power circuit of three phase boost converter with parallel arrangement.

Each phase of the boost converter is controlled by a pulse width modulation (PWM) signal where u_1, u_2, u_3 are taken from $\{0,1\}$. By using Kirchhoff's current law (KCL) and Kirchhoff's voltage law (KVL), the following equations can be extracted [39]:

$$\frac{di_{L1}}{dt} = -(1 - u_1) \frac{v_o}{L} - \frac{r_L}{L} i_{L1} + \frac{v_i}{L} \quad (5)$$

$$\frac{di_{L2}}{dt} = -(1 - u_2) \frac{v_o}{L} - \frac{r_L}{L} i_{L2} + \frac{v_i}{L} \quad (6)$$

$$\frac{di_{L3}}{dt} = -(1 - u_3) \frac{v_o}{L} - \frac{r_L}{L} i_{L3} + \frac{v_i}{L} \quad (7)$$

$$\frac{dv_o}{dt} = \frac{1}{C} [i_{L1}(1 - u_1) + i_{L2}(1 - u_2) + i_{L3}(1 - u_3)] - \frac{1}{RC} v_o \quad (8)$$

2.2.2. Average Model of the Three-Phase Boost Converter

Although the model presented by (5)–(8) is useful for simulating the power circuit, it is not applicable for designing the controller because it includes some binary control inputs (u_1, u_2, u_3). Generally, average model is used to design controller of such systems. In order to extract this model, first current of inductors and voltage of capacitor are considered as state variables and then by using (5)–(8) for more than one switching period (T_s), the average model is obtained as below [40–42]:

$$\bar{x} = \langle x \rangle = \frac{1}{T_s} \int_0^{T_s} x(t) dt$$

$$\dot{x}_1 = -(1 - D_1) \frac{1}{L} x_4 - \frac{r_L}{L} x_1 + \frac{f(x_I)}{L} \quad (9)$$

$$\dot{x}_2 = -(1 - D_2) \frac{1}{L} x_4 - \frac{r_L}{L} x_2 + \frac{f(x_I)}{L} \quad (10)$$

$$\dot{x}_3 = -(1 - D_3) \frac{1}{L} x_4 - \frac{r_L}{L} x_3 + \frac{f(x_I)}{L} \quad (11)$$

$$\dot{x}_4 = \frac{1}{C} x_F - \frac{1}{RC} x_4 - \frac{1}{C} (D_1 x_1 + D_2 x_2 + D_3 x_3) \quad (12)$$

$$x_I = x_1 + x_2 + x_3 \quad (13)$$

In above equations: $x_{1,2,3} = \langle i_{L1,2,3} \rangle$, $x_4 = \langle V_o \rangle$, $x_I = \langle i_T \rangle = \langle i_{fc} \rangle = \langle i_{pv} \rangle$, $D_j = \langle u_j \rangle$

2.3. Description of the Proposed Controller

The mathematical model proposed by above equations describes a nonlinear multi input-multi output (MIMO) system with parametric and nonparametric uncertainties, because the load resistance and V-I characteristic of micro sources are not deterministic. Control of such systems by using linear control methods might not be efficient [43,44]. Thus, in this section, a nonlinear robust controller that is based on sliding mode is proposed. For a better description, a block diagram of the system and location of the proposed controller using (5)–(8) is presented in Figure 4. This model which is associated to a three phase boost converter is controlled by a sliding mode based robust controller. As can be seen in the figure, in this controller, some feedbacks are taken from current of inductors and samples of input and output voltages are also applied to the controller as inputs. Outputs of this controller are binary signals that are finally applied to switches of the converter using PWM technique.

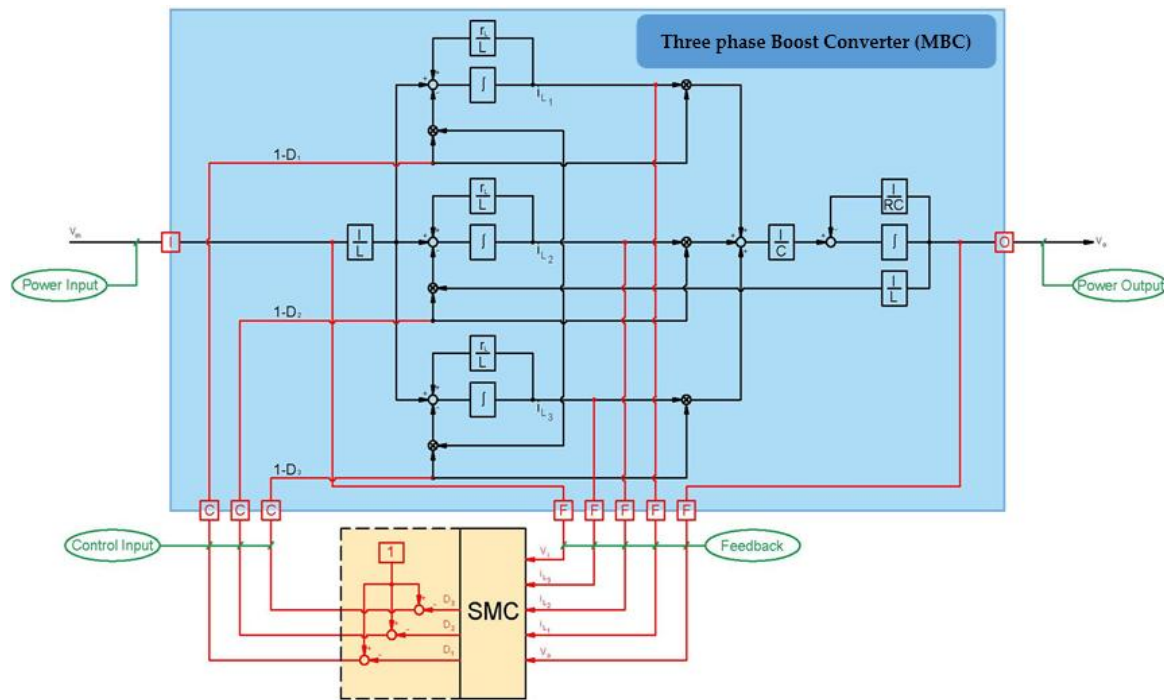


Figure 4. Block diagram of three phase boost converter with sliding mode controller (SMC).

Adaptive Sliding Mode Controller (ASMC)

Regarding to the above descriptions a controller based on sliding mode method with adaptive tuning module is presented because it is fully robust against uncertainties and provides the ability to estimate parameters in order to achieve control objectives. One of the main uncertainties is variations of the output load resistance. In order to overcome such uncertainty, controller should be more flexible and adaptable. Moreover, the controller should be able to estimate unknown parameters of the controlled system. At the beginning, resistance (R) and conductance (G) of the DC load is defined as follows:

$$\frac{1}{R} = G \quad (14)$$

If estimate of G is shown with \hat{G} , estimated error (\tilde{G}) can be described as follows:

$$\tilde{G} = G - \hat{G} \quad (15)$$

The purpose of the controller is to provide a constant output voltage in the condition where system has parametric uncertainty. To achieve this purpose the current (i_T) shall track a reference signal called x_{Id} . If in stable condition $i_T = x_{Id}$ and $v_o = V_{od}$, input power is equal to output power, where x_{Id} is related to V_{od} through the following equation (index d indicated desirable values of variables):

$$x_{Id} = \frac{V_{od}^2}{R \cdot f(x_{Id})} \stackrel{\text{def}}{=} \frac{V_{od}^2}{f(x_{Id})} G \quad (16)$$

This equation shows that current reference signal x_{Id} is related to uncertainty, and as this relation is not allowable in adaptive control methods. Here the current (i_T) is considered to track estimated reference signal \hat{x}_{Id} which is defined as below:

$$\hat{x}_{Id} = \frac{V_{od}^2}{f(\hat{x}_{Id})} \hat{G} \quad (17)$$

Because in (17) the reference path depends on the estimate of unknown system parameter (\hat{G}) so for better tracking in the presence of parameter uncertainty, sliding mode controller is used [37]. Since purpose of the controller is to current sharing among different phases, the sliding surface of each phase is defined as follows:

$$\begin{cases} s_1(x) = x_1 - \hat{x}_{1d} \\ s_2(x) = x_2 - \hat{x}_{2d} \\ s_3(x) = x_3 - \hat{x}_{3d} \end{cases} \quad (18)$$

where

$$\hat{x}_{1d} = \hat{x}_{2d} = \hat{x}_{3d} = \frac{1}{3}\hat{x}_{Id} = \frac{1}{3}\frac{V_{od}^2}{f(\hat{x}_{Id})}\hat{G} \quad (19)$$

The controller aims to deliver the system states to sliding surface $s = \dot{s} = 0$. When such purpose is satisfied, the system is in sliding mode. To obtain equivalent control energy, the derivative of sliding surface is considered zero.

$$s = \dot{s} = 0 \quad (20)$$

Using (18)–(20) and (9)–(11), equivalent control energy is obtained as follows:

$$\begin{cases} D_{1eq} = 1 + \frac{1}{x_4}(r_L x_1 - f(x_I) + L\hat{x}_{1d}) \\ D_{2eq} = 1 + \frac{1}{x_4}(r_L x_2 - f(x_I) + L\hat{x}_{2d}) \\ D_{3eq} = 1 + \frac{1}{x_4}(r_L x_3 - f(x_I) + L\hat{x}_{3d}) \end{cases} \quad (21)$$

In order to make the system robust against disturbances, a discontinuous term as follows is added to equations:

$$\begin{cases} D_1 = D_{1eq} + D_{1N} - \frac{L}{x_4}k_e e_{41} \\ D_2 = D_{2eq} + D_{2N} - \frac{L}{x_4}k_e e_{42} \\ D_3 = D_{3eq} + D_{3N} - \frac{L}{x_4}k_e e_{43} \end{cases} \quad (22)$$

where k_e is the first design parameter and D_{1N}, D_{2N}, D_{3N} are the discontinuous components which calculated as a design parameter as follows:

$$\begin{cases} D_{1N} = \frac{L}{x_4}\hat{D}_{1N} \\ D_{2N} = \frac{L}{x_4}\hat{D}_{2N} \\ D_{3N} = \frac{L}{x_4}\hat{D}_{3N} \end{cases} \quad (23)$$

If error between output voltage x_4 and desired value x_{4d} is called e_4 , it can be written as:

$$\begin{cases} e_{41} = x_4 - x_{4d1} \\ e_{42} = x_4 - x_{4d2} \\ e_{43} = x_4 - x_{4d3} \end{cases} \quad (24)$$

The desired value of x_{4d} is specified in the following. In (23), $\hat{D}_{1N}, \hat{D}_{2N}, \hat{D}_{3N}$ are additional inputs which are determined in the following.

The purpose of ASMC is changing the system states in order to equal the sliding surface to zero. For this purpose, it should be assured that the system is able to reach $s = \dot{s} = 0$ from any initial conditions as well as to remain in $s = 0$. Below Lyapunov function can meet above conditions:

$$V = \frac{1}{2}s^T s + \frac{1}{2}e_4^T e_2 + \frac{1}{2\gamma}\tilde{G}^2 \quad (25)$$

In which:

$$\begin{cases} s = [s_1, s_2, s_3]^T \\ e_4 = [e_{41}, e_{42}, e_{43}]^T \end{cases} \quad (26)$$

$\gamma > 0$ is adaptive gain. If time derivative of this function (\dot{V}) is negative definite, design objective which is asymptotic stability is achieved. Thus \dot{V} is obtained using (9)–(11) and (18) as follows:

$$\dot{V} = \frac{1}{L}[s_1(-(1-D_1)x_4) + s_2(-(1-D_2)x_4) + s_3(-(1-D_3)x_4) + 3f(x_I) - L\hat{x}_{Id}] + \frac{3}{\gamma}\tilde{G}\dot{\hat{G}} - (e_{41}\dot{e}_{41} + e_{42}\dot{e}_{42} + e_{43}\dot{e}_{43}) \quad (27)$$

Since $\tilde{G} = -\dot{\hat{G}}$, \dot{V} is negative definite. Using (21), (22) and (23), then (27) is obtained as follows:

$$\dot{V} = s_1D_{1N} + s_2D_{2N} + s_3D_{3N} + k_c(e_{41}^2 + e_{42}^2 + e_{43}^2) - \frac{\tilde{G}\dot{\hat{G}}}{\gamma} + e_{41}(\dot{e}_{41} - k_e s_1 + k_c e_{41}) + e_{42}(\dot{e}_{42} - k_e s_2 + k_c e_{42}) + e_{43}(\dot{e}_{43} - k_e s_3 + k_c e_{43}) \quad (28)$$

where $k_c > 0$ is the next design parameter. In (28) which has the state vector (s, e_4, \tilde{G}) , closed loop stability of the system can be observed by selecting \dot{D}_N , \dot{e}_4 and $\dot{\hat{G}}$. Therefor:

$$\begin{cases} \dot{D}_{1N} = -\alpha \cdot \text{sgn}(s_1) \\ \dot{D}_{2N} = -\alpha \cdot \text{sgn}(s_2) \\ \dot{D}_{3N} = -\alpha \cdot \text{sgn}(s_3) \end{cases} \quad (29)$$

$$\begin{cases} \dot{e}_{41} - k_e s_1 + k_c e_{41} + \frac{x_4}{C}\tilde{G} = 0 \\ \dot{e}_{42} - k_e s_2 + k_c e_{42} + \frac{x_4}{C}\tilde{G} = 0 \\ \dot{e}_{43} - k_e s_3 + k_c e_{43} + \frac{x_4}{C}\tilde{G} = 0 \end{cases} \quad (30)$$

$$\frac{\hat{G}}{\gamma} + \frac{x_4}{C}(e_{41} + e_{42} + e_{43}) = 0 \quad (31)$$

In the above equations, $\alpha > 0$ is a design constant. The larger is the coefficient α , error becomes zero rapidly, on the other hand, amplitude of the control input increases. Using (31), adaptive control law is obtained as follows:

$$\dot{\hat{G}} = -\frac{\gamma}{C}x_4(e_{41} + e_{42} + e_{43}) \quad (32)$$

Using (19) and (32) the time derivative of \hat{x} is:

$$\dot{\hat{x}}_{1d} = \dot{\hat{x}}_{2d} = \dot{\hat{x}}_{3d} = -\beta x_4(e_{41} + e_{42} + e_{43}) \quad (33)$$

$$\beta = \frac{1}{3C} \frac{V_{od}^2 \cdot \gamma}{f(\hat{x}_{Id}) + \frac{V_{od}^2 \cdot \hat{G} \cdot F(\hat{x}_{Id})}{f(\hat{x}_{Id})}} \quad (34)$$

where

$$F(\hat{x}_{Id}) = \left. \frac{df(x_I)}{dx} \right|_{x_I = \hat{x}_{Id}} \quad (35)$$

By merging (21), (22), (23) and (29):

$$\begin{cases} D_1 = 1 + \frac{L}{x_4} \left(\frac{r_L}{L} x_1 - \alpha \cdot \text{sgn}(s_1) - k_e(x_4 - x_{4d1}) - \frac{f(x_I)}{L} - \beta x_4(e_{41} + e_{42} + e_{43}) \right) \\ D_2 = 1 + \frac{L}{x_4} \left(\frac{r_L}{L} x_2 - \alpha \cdot \text{sgn}(s_2) - k_e(x_4 - x_{4d2}) - \frac{f(x_I)}{L} - \beta x_4(e_{41} + e_{42} + e_{43}) \right) \\ D_3 = 1 + \frac{L}{x_4} \left(\frac{r_L}{L} x_3 - \alpha \cdot \text{sgn}(s_3) - k_e(x_4 - x_{4d3}) - \frac{f(x_I)}{L} - \beta x_4(e_{41} + e_{42} + e_{43}) \right) \end{cases} \quad (36)$$

Dynamic of x_{4d} using (12), (14), (15), (24) and (30) is described as follows:

$$\begin{cases} \dot{x}_{4d1} = -k_e s_1 + k_c(x_4 - x_{4d1}) + \frac{x_F}{C} - \frac{\hat{G}}{C} - \frac{1}{C}(D_1 x_1 + D_2 x_2 + D_3 x_3) \\ \dot{x}_{4d2} = -k_e s_2 + k_c(x_4 - x_{4d2}) + \frac{x_F}{C} - \frac{\hat{G}}{C} - \frac{1}{C}(D_1 x_1 + D_2 x_2 + D_3 x_3) \\ \dot{x}_{4d3} = -k_e s_3 + k_c(x_4 - x_{4d3}) + \frac{x_F}{C} - \frac{\hat{G}}{C} - \frac{1}{C}(D_1 x_1 + D_2 x_2 + D_3 x_3) \end{cases} \quad (37)$$

Figure 5, shows block diagram of the proposed controller for one phase of the boost converter. In which control signal D is generated to be applied to the converter's switches. As can be seen from the above equations, control signal of each phase is determined considering the current of that phase which is affected by current of other phases, total current, input and output voltages and the control signal of other phases.

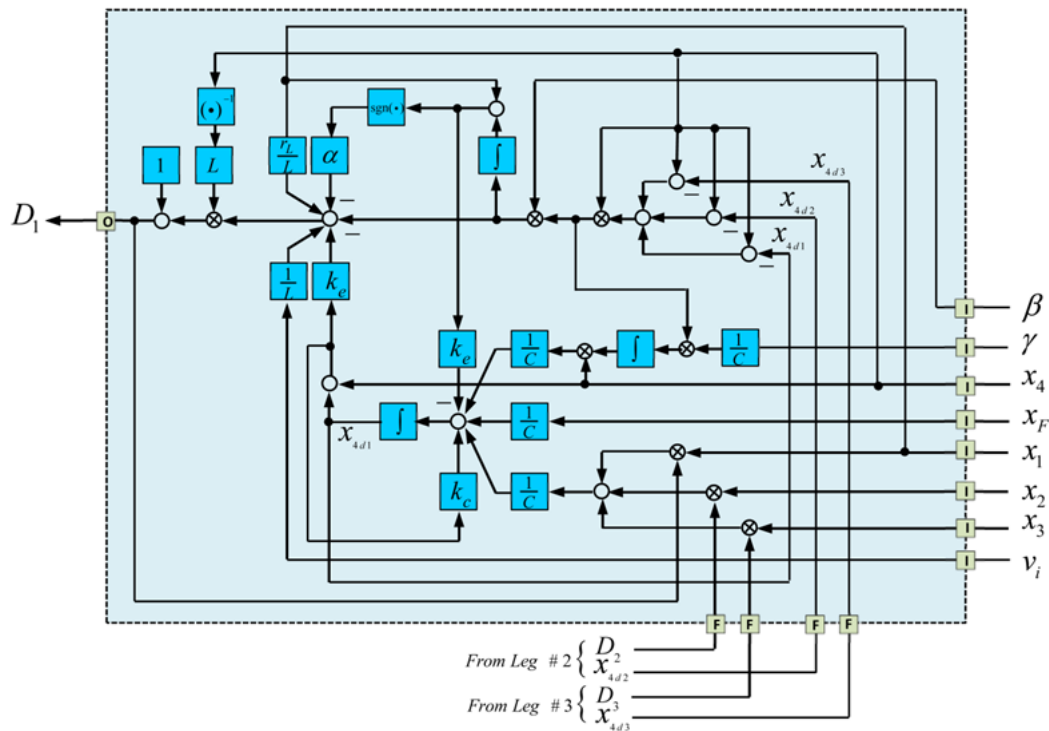


Figure 5. Realization of proposed sliding mode controller for each phase of boost converter.

3. Design of a Robust Controller in order to Improve Performance of AC Section

Many researches have been conducted for steady state operation and preserving dynamic stability of AC micro grids. In most studies, droop control method is presented as an effective method [14–18]. In conventional droop control, small signal stability is provided by adjusting frequency and voltage droop coefficients and enhancing power sharing among micro-grids [15,16]. If droop coefficients in island mode are increased, power sharing correctness is enhanced at the expense of reducing accuracy of frequency and voltage regulation. Larger droop coefficients create negative effect on system stability as well as limitations on operational performance. In other words, there is a trade-off among power distribution, power quality, transient response and system stability. However, in many disturbances especially large signal disturbances, the inefficiency of the droop control method is obvious.

3.1. Structure of the Proposed Controller in AC Section

In order to solve the mentioned issues, an inclusive control structure is proposed. Each of the control necessities of AC section of a micro-grid in steady and transient states are presented in this structure. This structure includes power, frequency and angle control loops and benefits from all of the

advantages of them concurrently. Invariant frequency utilization and accrued power distributing can be achieved using frequency droop while transient stability is provided by the proposed supplement controller which is a nonlinear controller. Other advantages of proposed control structure will be described later.

3.2. Modeling AC Section of the Micro-Grid

In this paper, a general framework is used to design and establish a controller for both operation modes. To this end, first a model is proposed to improve dynamic of the inertia less converters based on virtual rotor idea by imitating inertia of the rotor and damping coefficient of the synchronous generators. This model which is described completely in [45–47] and introduced as a virtual synchronous machine (VISMA), models a power electronic converter the same as Figure 6a, similar to a synchronous generator.

First idea of this model is to imitate back induction voltage law and dynamic of rotor of the synchronous generator with momentum J and viscose friction m . The advantages of imitating rotor dynamic are improving dynamic response of the converter and creating a proper control structure to exploit all of the operating conditions. In this model, the virtual rotor is a frequency dynamic controller, a role that does not exist in conventional voltage/current controller. Virtual friction (m) damps frequency oscillations. Summary of the modeling based on VISMA using equation of the voltage generated by conventional synchronous generator is as follows [45]:

$$\tilde{e} = \lambda_F \dot{\theta} \sin \tilde{\theta} \quad (38)$$

where \tilde{e} shows a balanced three phase voltage, λ_F is excitation flux, θ and $\dot{\theta}$ are virtual angle and angular speed. Frequency dynamic can be presented as follows:

$$J\ddot{\theta} = T_m - T_e - T_D = T_m - T_e - K_p\dot{\theta} \quad (39)$$

In (39), K_p is damping ratio, T_m and T_e are virtual mechanical and electromagnetic torques. T_e is calculated based on stored energy in magnetic field of the machine (W_{fld}) as follows:

$$T_e = \left. \frac{\partial W_{fld}}{\partial \theta} \right|_{\lambda_F = \text{constant}} \quad (40)$$

By defining W_{fld} in terms of current and flux of the armature and exciter (40) is obtained as follows:

$$T_e = \frac{3}{2} \lambda_F i \cos \delta \quad (41)$$

In addition, active and reactive powers can be described as follows:

$$P = \frac{3}{2} \dot{\theta} \lambda_F i \cos \delta \quad (42)$$

$$Q = \frac{3}{2} \dot{\theta} \lambda_F i \sin \delta \quad (43)$$

In this model state variables include current of inductors (i), voltage of capacitor (v), virtual angle and angular speed (θ and $\dot{\theta}$). Also mechanical torque (T_m) and excitation flux (λ_F) are control inputs.

For proper operation of converter based on this model, a controller is required which can follow proper values of active and reactive powers as well as increase system stability by generating appropriate torque and flux signals.

Same as synchronous generators, in VISMA frequency droop is used to improve power sharing and frequency restoration. In this modeling, the frequency droop is defined as follows:

$$K_p = -\frac{\Delta P}{\Delta \dot{\theta}} \quad (44)$$

Similarly, voltage droop can be defined as follows:

$$K_q = -\frac{\Delta Q}{\Delta V} \quad (45)$$

Considering the above descriptions, the model of AC converters in this paper can be presented as Figure 6b [45].

As can be seen in Figure 6b, this model has a real power control loop and is able to share power variations with other similar converters and same size synchronous generators automatically due to internal frequency droop mechanism. It can also be said that due to absence of mechanical equipment, structure of this loop is very simple.

Frequency droop loop (with gain K_p) has a time constant of $T_F = 1/K_p$. Thus, if T_F is selected as a design parameter, J can be obtained as follows:

$$J = K_p \cdot T_F \quad (46)$$

Lower loop is related to reactive power control. Error between reference voltage and output voltage is multiplied by the droop coefficient K_q and is summed up with error between output reactive power (Equation (43)) and its reference value finally the result (u_d) is obtained as excitation flux after passing integrator with gain $1/K$. Voltage droop loop (with gain K_q) has a time constant approximately equal to $T_V = \frac{K}{\theta K_q} = \frac{K}{\theta_n K_q}$. Thus, if T_V is selected as a design parameter, K can be obtained as follows:

$$K = T_V \dot{\theta}_n K_q \quad (47)$$

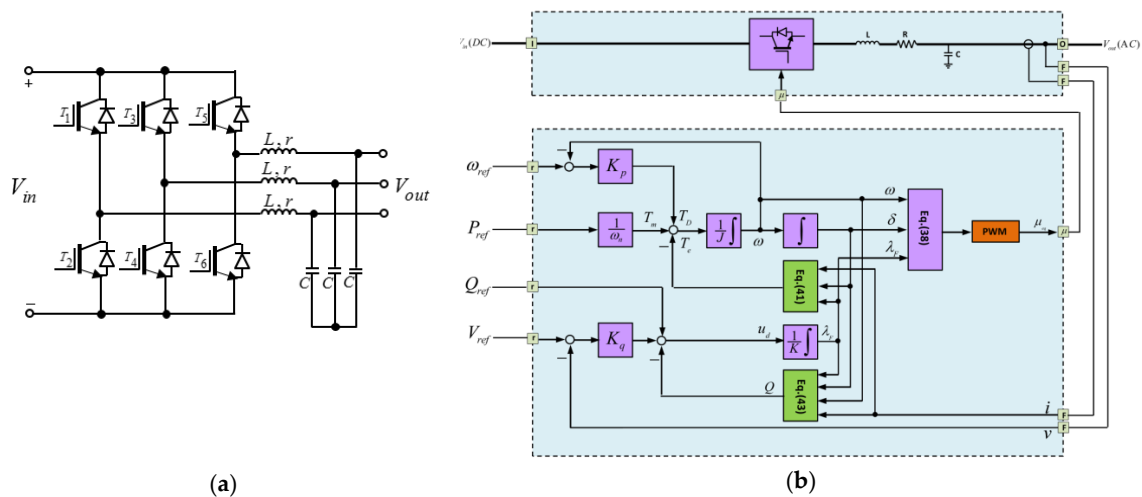


Figure 6. (a) Power circuit of DC/AC converter; (b) controller model of converter based on VISMA.

3.3. Adaptive-Nonlinear Supplement Control

Since the model based on VISMA performs well in steady and dynamic states and resolves operational requirements, but it does not perform well in large signal disturbances such that the system under this model becomes unstable. Thus, in this paper, a supplement nonlinear controller is added to the existing droop controller to guarantee transient stability of the converter (and micro-grid).

In fact, when a large disturbance occurs, the proposed nonlinear controller injects an additional signal to the VISMA to stabilize the system by changing amplitude of the virtual flux. In steady state, this controller is in idle phase. Advantages of the proposed controller include:

- Universal and flexible structure for all of the operation modes and not requiring to change strategy after islanding detection.
- As compared to other controllers, where delay in islanding detection reduces stability margin, this problem is resolved inherently in the proposed controller.
- Possibility to create a soft and seamless path from grid connected mode to islanding mode.
- Frequency droop control loop of this controller is a useful tool for power sharing between micro sources.
- This controller only uses local signals, thus no communication infrastructure is required.

Figure 7 shows the structure of the supplementary nonlinear controller. According to this figure, it is obvious that the supplement controller adds an extra command (u_{ax}) to the VISMA model which aims to improve stability.

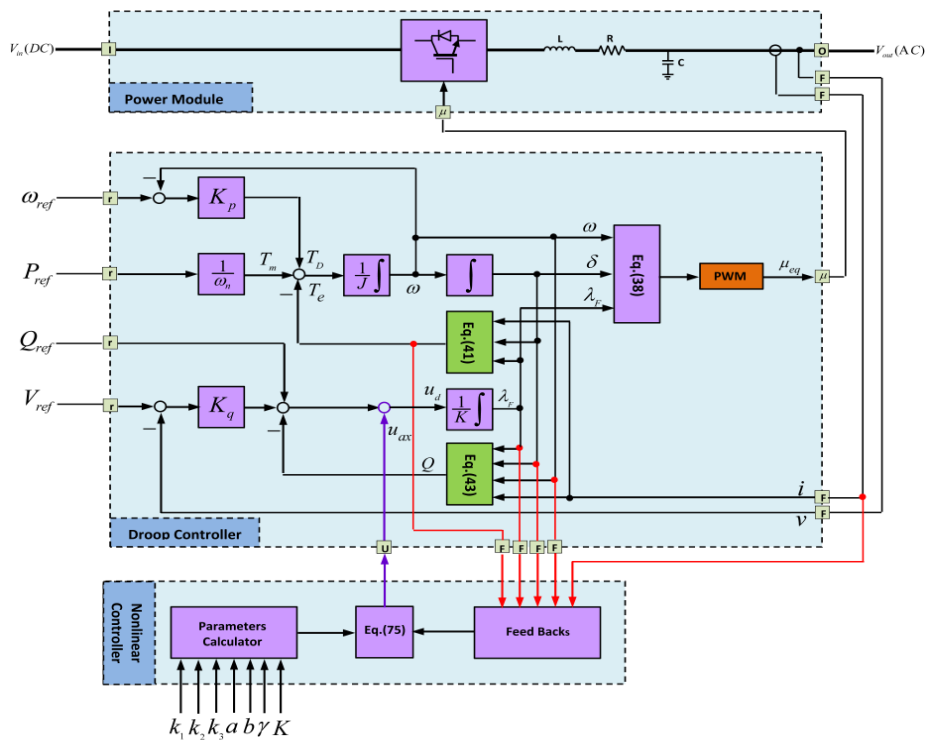


Figure 7. Location of proposed controller on VISMA model.

Finally, it can be said that stable performance of the micro-grid during a harsh transient like unplanned islanding, short circuit and sudden changes in power consumption is satisfied using this controller.

In the proposed controller, power angle (δ), frequency (ω) and virtual torque (T_e) are state variables. Frequency dynamic is controlled by frequency droop control and virtual rotor as shown in Figure 7. Accordingly, dynamics of angle and frequency can be described as follows.

$$\Delta \dot{\delta} = \Delta \omega \quad (48)$$

$$\Delta \dot{\omega} = -\frac{m}{J} \Delta \omega + \frac{1}{J} (-T_e + T_{ref}) \quad (49)$$

In (48) and (49), $\Delta\delta$ and $\Delta\omega$ represent frequency and angle deviations from their work point. Dynamic of the torque equation is calculated using the following equation:

$$T_e = \frac{3}{2} \dot{\lambda}_F i \cos \delta + \frac{3}{2} \lambda_F \dot{i} \cos \delta - \frac{3}{2} \lambda_F i \Delta\omega \sin \delta \quad (50)$$

Derivative of flux is determined using dynamic of the voltage loop of Figure 7. In order to design this controller, following state space model is used:

$$\begin{cases} \dot{x}_1 = x_2 \\ \dot{x}_2 = ax_2 + bx_3 \\ \dot{x}_3 = u_{ax} + \frac{3}{2} \left(\lambda_f \dot{i} \cos x_1 - \lambda_f i x_2 \sin x_1 \right) + \Psi \end{cases} \quad (51)$$

In this equation, $x_1 = \Delta\delta$, $x_2 = \Delta\omega$, $x_3 = \Delta T_e$, $a = -\frac{m}{J}$, $b = -\frac{1}{J}$ and:

$$u_{ax} = \frac{3}{2K} u_d \cos x_1 \quad (52)$$

u_d is the main input of virtual flux generator or input of the integrator of the reactive power control loop as shown in Figure 7 and u_{ax} is the supplementary signal provided by proposed supplementary nonlinear controller. Term Ψ is introduced to consider system uncertainty which can be caused by disturbances, variations in model parameters, inaccurate measurements, etc. This uncertainty is usually estimated by adaptive techniques to be robust against mentioned uncertainties. Purpose of the controller is to minimize error between desired reference value x_{1ref} and its real value x_1 . Error is defined as follows:

$$e_i = x_i - x_{iref} \quad (53)$$

Below Lyapunov function is defined to design this controller:

$$V_1 = \frac{1}{2} e_1^2 \quad (54)$$

Derivative of this equation is equal to:

$$\dot{V}_1 = e_1 \dot{e}_1 \quad (55)$$

In order to stabilize state x_1 , derivative of V_1 should be negative definite. Thus:

$$x_{2ref} = -k_1 e_1, \quad k_1 > 0 \quad (56)$$

In which:

$$\dot{V}_1 = -k_1 e_1^2 + e_1 e_2 \quad (57)$$

According to (57) there is no guarantee that \dot{V}_1 is negative definite. In next steps, \dot{V}_1 becomes negative by proper selection of x_{3ref} and u_d . In order to stabilize frequency dynamic, x_{3ref} is selected according to Lyapunov function.

$$V_2 = V_1 + \frac{1}{2} e_2^2 \quad (58)$$

Derivative of (59) is equal to:

$$\dot{V}_2 = \dot{V}_1 + e_2 \dot{e}_2 \quad (59)$$

where $\dot{e}_2 = \dot{x}_2 - \dot{x}_{2ref}$. Using (51) and (56), we have:

$$\dot{e}_2 = [1 - k_1(a + k_1)]e_1 + (a + k_1)e_2 + be_3 + bx_{3ref} \quad (60)$$

Thus \dot{V}_2 is simplified as follows:

$$\dot{V}_2 = -k_1 e_1^2 + \left[b x_{3ref} - (k_1^2 + k_1 b - 1) e_1 + (a + k_1) e_2 \right] e_2 + b e_2 e_3 \quad (61)$$

Now, if

$$x_{3ref} = c_1 e_1 + c_2 e_2 \quad (62)$$

In which

$$\begin{cases} c_1 = -\frac{1-k_1(a+k_1)}{b} \\ c_2 = -\frac{k_1+k_2+a}{b} \end{cases} \quad (63)$$

Thus:

$$\dot{V}_2 = -k_1 e_1^2 - k_2 e_2^2 + a e_2 e_3 \quad (64)$$

In order to guarantee stability of the system, the final Lyapunov function is considered as:

$$V_3 = V_2 + \frac{1}{2} e_3^2 + \frac{1}{2} \gamma (\Psi - \hat{\Psi})^2 \quad (65)$$

In which $\hat{\Psi}$ is an estimate of uncertainty function Ψ and γ is gain of the adaptive rule. Dynamics of e_3 can be written as follows using associated equations:

$$\dot{e}_3 = \dot{x}_3 - \dot{x}_{3ref.} = u_{ax} + \frac{3}{2} \left(\lambda_f \dot{i} \cos x_1 - \lambda_f i x_2 \sin x_1 \right) + \Psi - \dot{x}_{3ref.} \quad (66)$$

Value of x_{3ref} can be found as follows using (51), (56) and (62):

$$x_{3ref.} = c_1 \dot{e}_1 + c_2 \dot{e}_2 \quad (67)$$

In which:

$$\dot{e}_2 = \dot{x}_2 - \dot{x}_{2ref.} = a x_2 + b x_3 + k_1 \dot{e}_1 = a x_2 + b x_3 + k_1 x_2 \quad (68)$$

Finally, x_{3ref} is obtained as follows

$$\dot{x}_{3ref.} = A_1 e_1 + A_2 e_2 + b c_2 e_3 \quad (69)$$

$$\begin{cases} A_1 = b c_1 c_2 - k_1 (c_1 + k_1 c_2 + a c_2) \\ A_2 = c_1 + b c_2^2 + a c_2 + k_1 c_2 \end{cases} \quad (70)$$

Thus, \dot{V}_3 is equal to

$$\begin{aligned} \dot{V}_3 = & -k_1 e_1^2 - k_2 e_2^2 + \left[u_{ax} - \frac{3}{2} \lambda_f \dot{i} \cos x_1 - \left(A_1 - \frac{3}{2} k_1 \lambda_f i \sin x_1 \right) e_1 \right. \\ & \left. - \left(-b + A_2 + \frac{3}{2} \lambda_f i \sin x_1 \right) e_2 - b c_2 e_3 + \theta \right] e_3 - \gamma (\Psi - \hat{\Psi}) \dot{\hat{\Psi}} \end{aligned} \quad (71)$$

Now, if adaptation rule is selected as:

$$\dot{\hat{\Psi}} = \frac{1}{\gamma} e_3 \quad (72)$$

Then:

$$\begin{aligned} \dot{V}_3 = & -k_1 e_1^2 - k_2 e_2^2 + \left[u_{ax} - \frac{3}{2} \lambda_f \dot{i} \cos x_1 - \left(A_1 - \frac{3}{2} k_1 \lambda_f i \sin x_1 \right) e_1 \right. \\ & \left. - \left(-b + A_2 + \frac{3}{2} \lambda_f i \sin x_1 \right) e_2 - b c_2 e_3 + \hat{\Psi} \right] e_3 \end{aligned} \quad (73)$$

Accordingly, if control input is selected as follows:

$$u_{ax} = -\frac{3}{2}\lambda_f \dot{i} \cos x_1 - \left(A_1 - \frac{3}{2}k_1\lambda_f i \sin x_1\right)e_1 + \left(-b + A_2 + \frac{3}{2}\lambda_f i \sin x_1\right)e_2 - (bc_2 - k_3)e_3 + \dot{\Psi} \quad (74)$$

By displacing (73) in (74), Lyapunov function is described as below:

$$\dot{V}_3 = -k_1 e_1^2 - k_2 e_2^2 - k_3 e_3^2 \quad (75)$$

Therefore, the stability of the system is guaranteed when using control signal in (74). Control parameters of this controller are $[k_1, k_2, k_3, \gamma]$. Performance of the system depends on these coefficients and designer has a high degree of freedom to find the best combination of these constants to obtain the maximum trade-off between performance objectives of the system. Realization of proposed controller for AC side of the microgrid is shown in Figure 8.

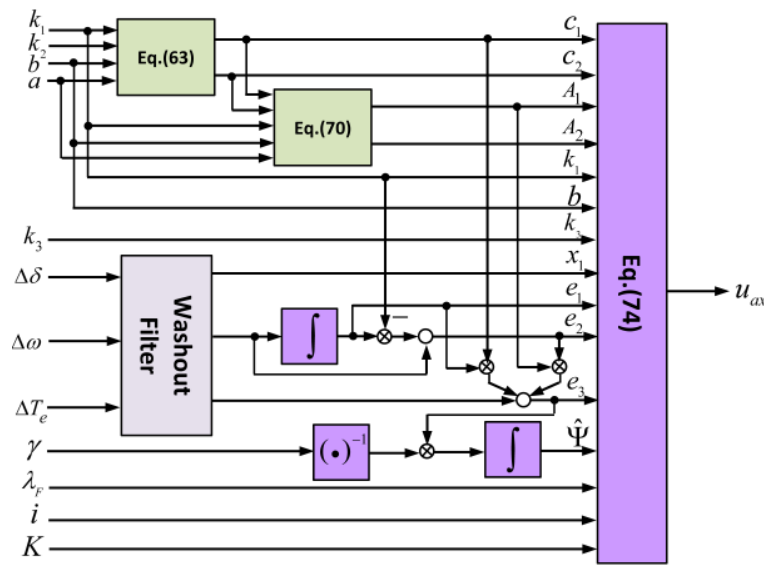


Figure 8. Realization of proposed controller of AC side.

4. Simulation Results and Evaluation of the Proposed Controller

Different simulations are performed in MATLAB/SIMULINK (MathWorks Inc., Natick, MA, USA) to study dynamic and static performances of the proposed controller topologies. These scenarios include:

- Unspecified changes in the current taken from DC bus of each micro-sources
- Changing electrical characteristic of the micro- sources
- Unplanned islanding
- Loading in islanding mode
- Short circuit in PCC

The simulated system shown in Figure 9 has three micro-generators that provide their local load in parallel and supply other common loads in PCC. Parameters of the micro-generators and the related network are given in Table A1. Input voltage of inverters is fully stabilized using the proposed control topology of related boost converter. Input sources are DC and include fuel cell and photo voltaic panel. Dynamic characteristic of these sources are completely considered in the simulations.

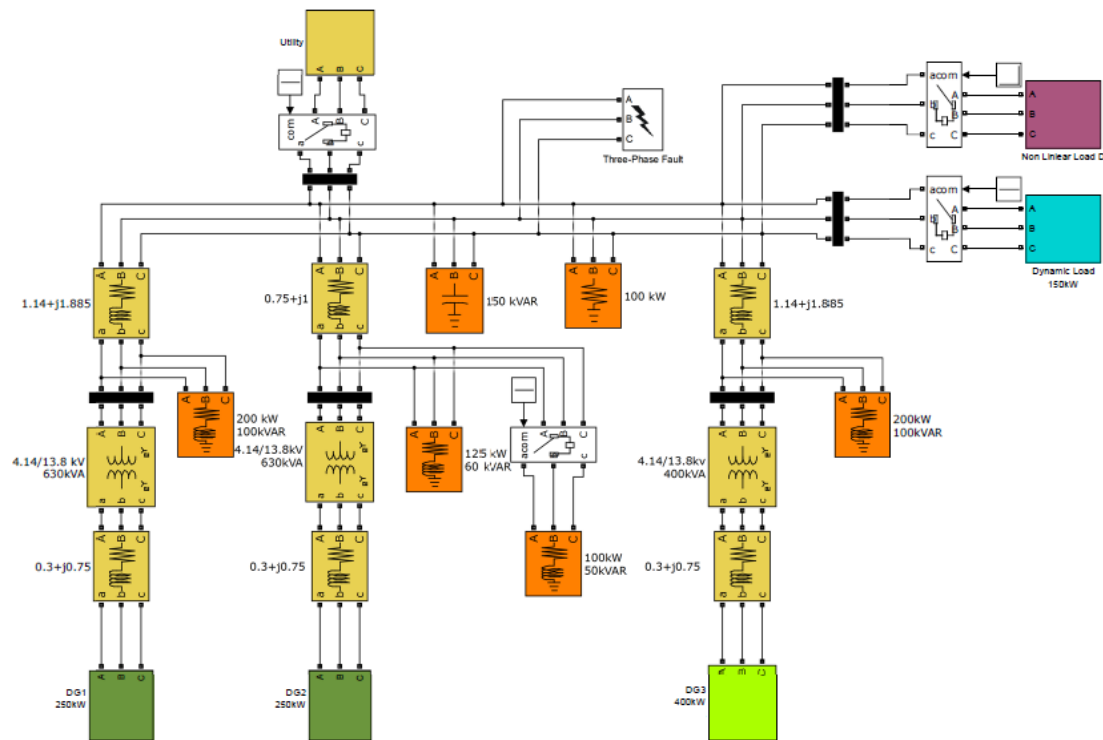


Figure 9. Simulation of micro grid by MATLAB/SIMULINK software (R2014a).

4.1. Unspecified Changes in the Current Taken from DC Bus

In this scenario, resistance of the connected load to output of the boost converter varies as steps with different amplitudes and purpose of the controller is to stabilize voltage of DC bus on the reference value. For this purpose, according to Figure 10a, the resistance of the load is changed as steps with different amplitudes. First, the identification section of the proposed controller estimates the load conductance at each moment rapidly according to Figure 10b, such that error of this estimate tends towards zero. Result of this fast estimate at first stage is to change duty cycle of switches according to Figure 10c. Chattering phenomenon which is one of the characteristics of sliding mode controller is seen clearly in this figure.

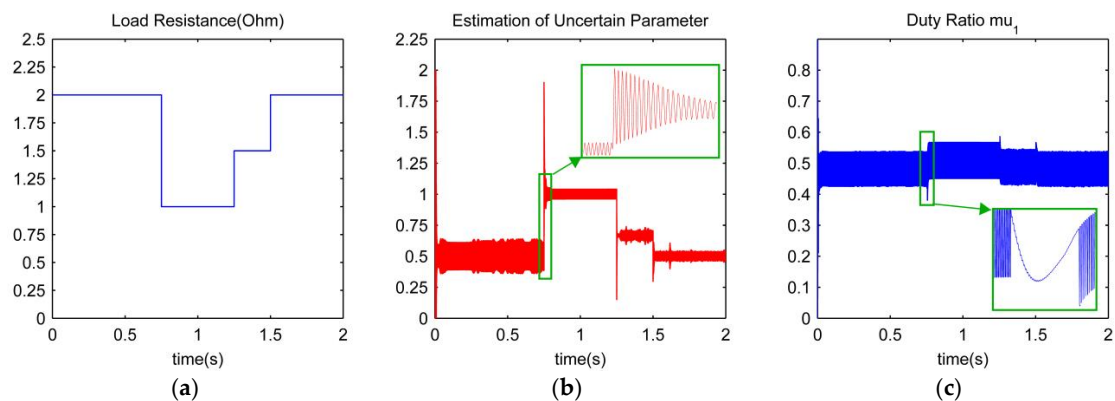


Figure 10. (a) Variation of DC load resistance; (b) Estimation of load conductance; (c) Duty cycle of switches created by proposed controller.

Figure 11b shows the voltage of the fuel cell while changing the load. According to this figure, due to dynamic of the V-I characteristic of cells, severe variation is observed in generated voltage of the fuel cell. Although voltage of the fuel cell varies significantly, but according to Figure 11a in the

presence of the proposed controller, the output voltage of the converter is stabilized on the defined value (480 V). This figure shows the high proficiency of the proposed controller. Figure 11c shows current of different phases as well as current taken from fuel cell. According to this figure, current sharing between different phases is done very well and one-third of the total current has passed through each phase. One of the main advantages of multiphase boost converter which is eliminating ripple of the current taken from the fuel cell can be seen in this figure. This issue is very important as increases the lifetime of the cell.

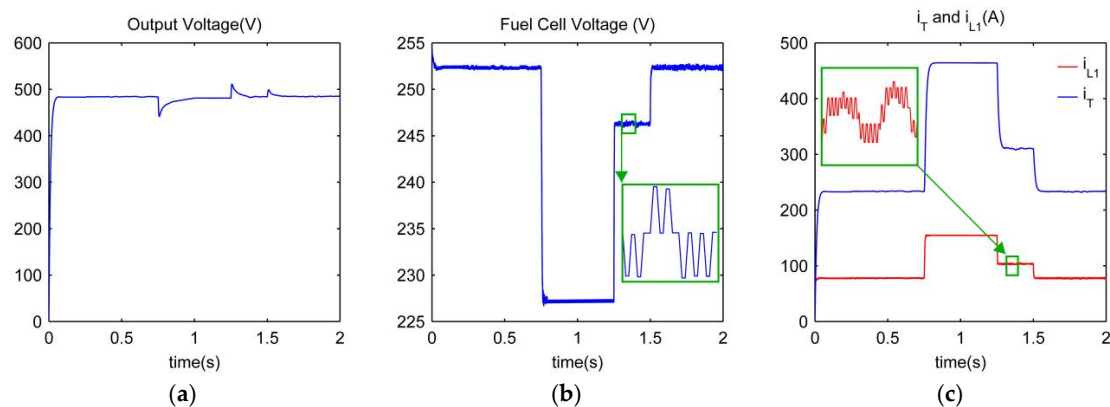


Figure 11. Responses of DC side of the hybrid micro grid (a) Output voltage; (b) Fuel cell voltage; (c) Phase current of boost converter and fuel cell current.

4.2. Changing Electric Characteristic of the Micro-Source

Since the electric characteristic of micro-sources are uncertain due to changes in environmental conditions, robustness of the proposed converter against this uncertainty should be evaluated. For this purpose, the dynamic characteristic of the cell is varied 10% according to Figure 12a and the previous scenario, changing resistance subsequently, is performed again. In the presence of such uncertainty, although fuel cell as input of the converter has changed as shown in Figure 12b, but in the presence of the proposed controller, the system is able to adjust output voltage as in Figure 12c. Finally, it can be said that this scenario shows high performances as well as high robustness of the proposed controller in the presence of uncertainty in the load and source characteristics which results in a fully stable DC bus in the network and possibility of AC voltage regulation in hybrid micro grid consequently. Similar results and analysis are obtained for input of the photo voltaic panels, but they are not presented in this paper due to limited number of pages.

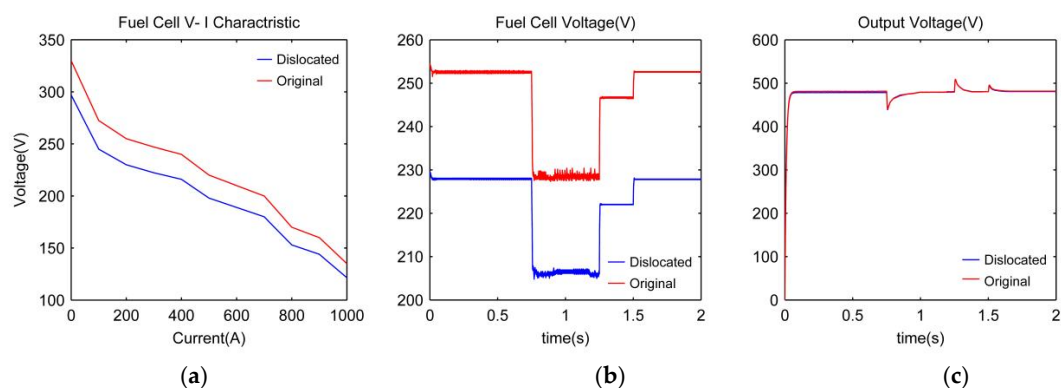


Figure 12. Robustness check of proposed controller (a) Changing of V-I characteristic of fuel cell; (b) Fuel cell voltage regard changing characteristic; (c) Output voltage regard changing characteristic.

4.3. Unplanned Islanding

It is assumed that DG units are connected in parallel in a period of time and all of them are connected to the utility. At $t = 1$ s, islanding occurs and micro-grid is separated from the utility. Islanding is a large disturbance from controller's point of view. Figures 13–15 show variations of power, voltage and frequency during transition from grid connected mode to autonomous mode.

Since in the studied system, it is assumed that one portion of the load power is provided by the utility, output power of DGs increases to provide local load. This scenario is one of the most difficult states which might occur while operating a micro-grid.

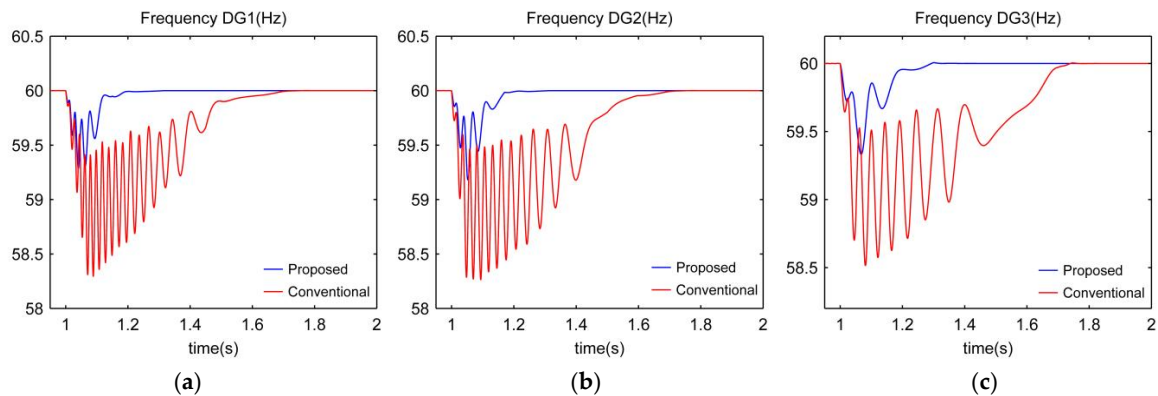


Figure 13. Frequency response of DG's during islanding using proposed supplementary control compare with conventional droop controller (a) DG1; (b) DG2; and (c) DG3.

Results show a soft transition with minimum overshoot in variables as compared to their steady state, such that average damping time of frequency variations is about 200 ms and maximum undershoot is 0.7 Hz. Voltage of DG units are shown in Figure 14. Based on this figure the damping time and maximum under/overshoot of the DG's output voltages by using proposed controller are very negligible in compare with conventional droop controller.

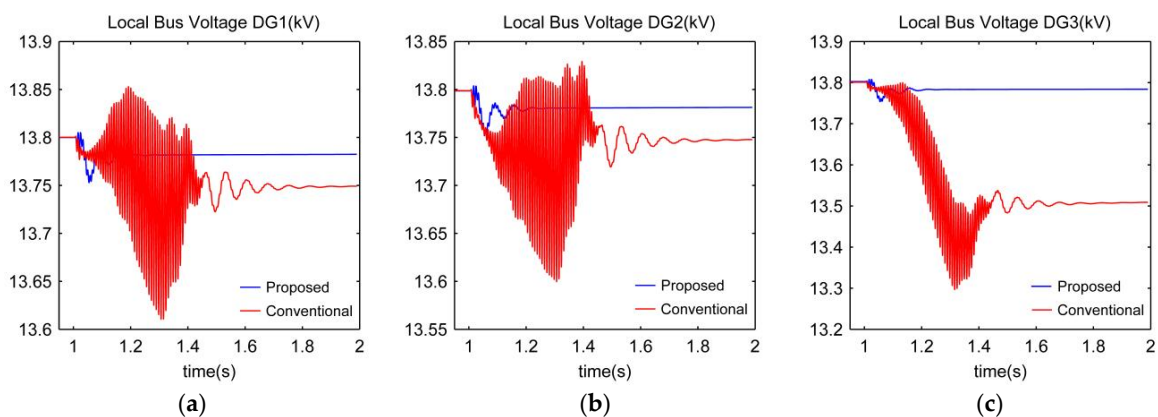


Figure 14. Voltage response of DG's during islanding using proposed supplementary control compare with conventional droop controller (a) DG1; (b) DG2; and (c) DG3.

Power sharing in the presence of proposed nonlinear controller is shown in Figure 15 which has occurred with softer transitions.

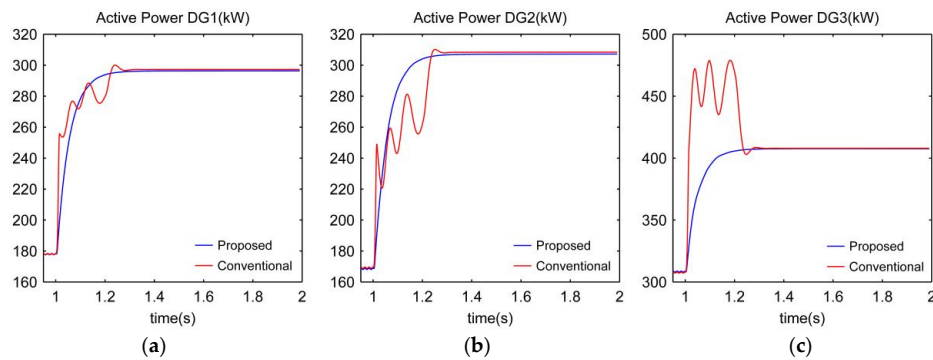


Figure 15. Power sharing of DG's during islanding using proposed supplementary control compare with conventional droop controller (a) DG1; (b) DG2; and (c) DG3.

4.4. Loading in Islanding Mode

In this case, it is assumed that micro-grid operates in islanding mode and at $t = 1$ s, a 125 kW nonlinear load in PCC is connected to it. Simulation results are given in Figures 16–18.

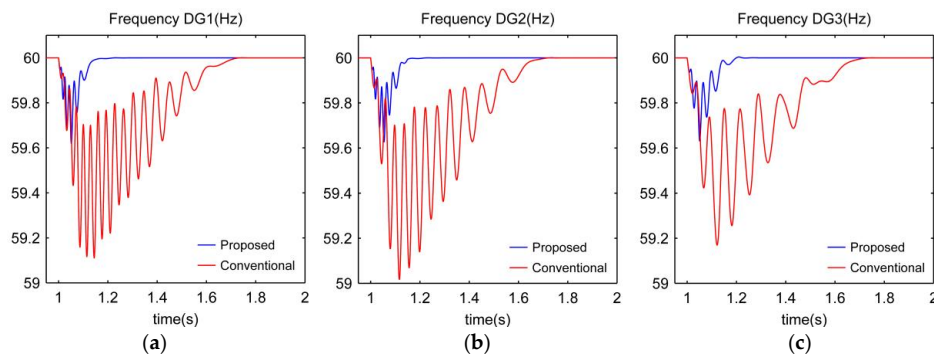


Figure 16. Frequency response of DG's in load impact condition using proposed supplementary control compare with conventional droop controller (a) DG1; (b) DG2; and (c) DG3.

According to these results, when applying a nonlinear load, the proposed controller can reconfigure the network and accelerate damping of variables oscillations such that frequency restoration is performed in less than 150 ms and maximum frequency drop is 0.35 Hz.

Based on Figure 17 the damping time and maximum under/overshoot of the DG's output voltages by using proposed controller are very negligible in compare with conventional controller.

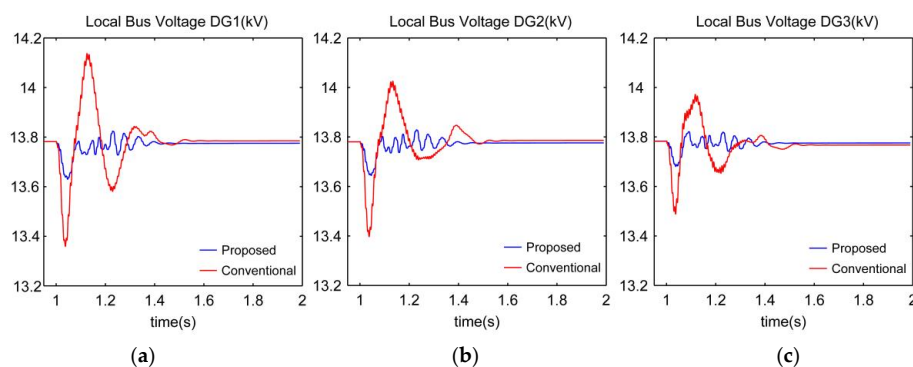


Figure 17. Voltage response of DG's in load impact condition using proposed supplementary control compare with conventional droop controller (a) DG1; (b) DG2; and (c) DG3.

It can also be seen that power sharing between micro-sources in the presence of the proposed controller is very soft while in the presence of conventional drop control, overshoot is observed.

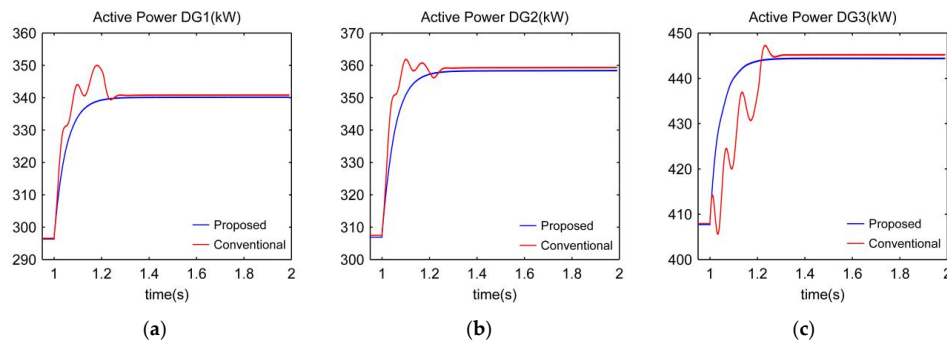


Figure 18. Power sharing of DG's in load impact condition using proposed supplementary control compare with conventional droop controller (a) DG1; (b) DG2; and (c) DG3.

4.5. Short Circuit in PCC

At $t = 1$ s, a three phase symmetric short circuit fault occurs in PCC, because of which after 250 ms, fault is cleared and islanding mode has occurred. According to the results shown in Figures 19–21, it can be seen that while fault is established, frequency drops 1 Hz and when fault is resolved, 1.5 Hz overshoot is created and after 300 ms, frequency is restored very well.

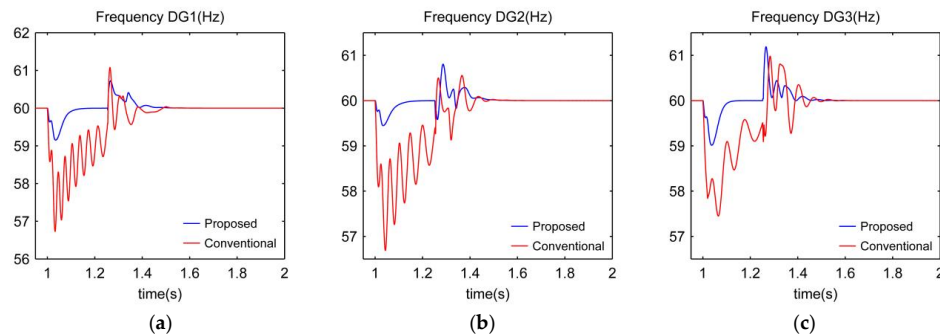


Figure 19. Frequency response of DG's in short circuit condition using proposed supplementary control compare with conventional droop controller (a) DG1; (b) DG2; and (c) DG3.

As shown in Figure 20 while fault persists, the voltage in PCC is zero and has the minimum possible value at the output of micro-sources. After clearing fault, when the proposed controller is available, voltage is restored with appropriate overshoot and settling time.

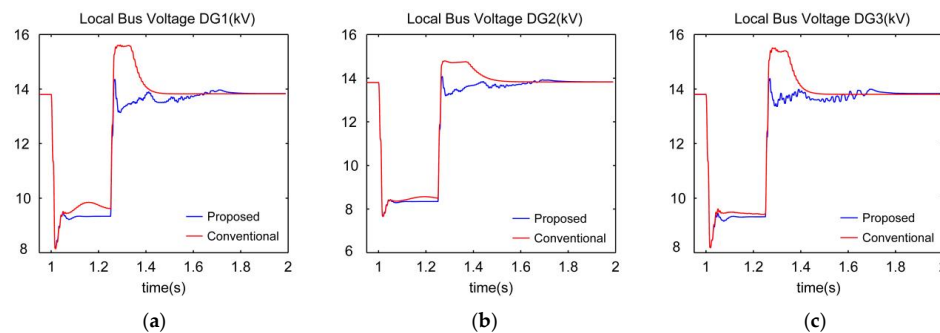


Figure 20. Voltage response of DG's in short circuit condition using proposed supplementary control compare with conventional droop controller (a) DG1; (b) DG2; and (c) DG3.

As shown in Figure 21, power distribution during short circuit is better in the presence of the proposed controller as compared to conventional controller. In the presence of the nonlinear controller, power injection to fault point is limited.

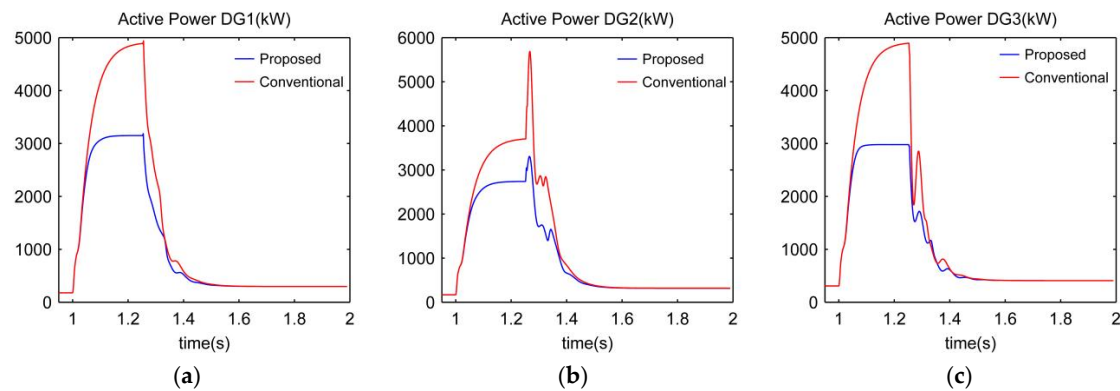


Figure 21. Power of DG units in short circuit condition using proposed supplementary control compare with conventional droop controller (a) DG1; (b) DG2; and (c) DG3.

5. Conclusions

In this paper, a flexible and efficient integrated controller is proposed to improve the performance of the hybrid micro-grid. First, voltage of the DC link is stabilized well by applying the proposed control strategy to the input boost converter, and then the proposed controller is applied to the output converter to stabilize the voltage and frequency and so satisfy all control and management requirements of the micro-grid in steady state and dynamic state. Due to the nonlinear nature of the proposed controller, large signal stability in the presence of the most severe fault, namely three phase short circuit in PCC is guaranteed. The main reason of efficiency of the proposed controller is to add an extra command to the virtual flux calculator of the output VISMA based model converters. The proposed strategy not only has a high reliability but it also does not require any communication infrastructures which are directly resulted from using local information. Investigating simulation results of the proposed controller shows that stability margin and flexibility of exploiting hybrid micro-grids using this controller is high which increases penetration of these micro-sources in future intelligent networks.

Author Contributions: Reza Pejmanfar is the main author of this work. This paper further elaborates on some of the results from his Ph.D. dissertation. Mahmoud Reza Haghifam supervised the project and supported Reza Pejmanfar's research in terms of both scientific and technical expertise. Soodabeh Soleymani and Babak Tavassoli assisted in the results analysis and interpretation. The manuscript was written by Reza Pejmanfar and was reviewed and revised by Mahmoud Reza Haghifam.

Conflicts of Interest: The authors declare no conflict of interest.

Appendix A

Parameters of the input and output converters, proposed controllers and general information of the micro-grid employed in simulations are given in Table A1.

Table A1. System Parameters.

Parameters		DG1	DG2	DG3
Voltage (V)	Local Bus		480	
	PCC		13,800	
Power (kW)	Rated Power	250	250	400
	Local Load	200	125	200
	Common Load		100	
		Static	150	
		Dynamic Non Linear	125	
Time Constants (S)	Voltage Loop	0.01	0.01	0.01
	Power Loop	0.04	0.04	0.04
Gains	Frequency Droop (Kp)	40	40	53
	Voltage Droop (Kq)	0.0016	0.0016	0.0017
	Virtual Flux Integrator	0.045	0.045	0.045
Power Angle Reference (rad)		0.2	0.2	0.3
Resistance (Ohm)	Out Put Filter	0.2	0.2	0.2
	Transformer	0.25	0.25	0.25
	Line	1.14	0.75	1.14
Inductance (mH)	Out Put Filter	3	3	3
	Transformer	3.25	3.25	3.25
	Line	5	2.65	5
DC/DC Boost Converter	L(mH)/R(mΩ)/C(μF)		2.2/20/1200	
	Switching Frequency (kHz)		10	
	Adaption Gains		$k_e = 400/k_c = 1000/\alpha = 1200$	

References

- Ding, G.; Gao, F.; Zhang, F. Control of hybrid AC/DC microgrid under islanding operational conditions. *J. Mod. Power Syst. Clean Energy* **2014**, *2*, 223–232. [\[CrossRef\]](#)
- Blaabjerg, F.; Zhe, C.; Kjaer, S.B. Power electronics as efficient interface in dispersed power generation systems. *IEEE Trans. Power Electron.* **2004**, *19*, 1184–1194. [\[CrossRef\]](#)
- Baran, M.E.; Mahajan, N.R. DC distribution for industrial systems: Opportunities and challenges. *IEEE Trans. Ind. Appl.* **2003**, *39*, 1596–1601. [\[CrossRef\]](#)
- Sannino, A.; Postiglione, G.; Bollen, M.H. Feasibility of a DC network for commercial facilities. *IEEE Trans. Ind. Appl.* **2003**, *39*, 1499–1507. [\[CrossRef\]](#)
- Carrasco, J.M.; Franquelo, L.G.; Bialasiewicz, J.T. Power electronic systems for the grid integration of renewable energy sources: A survey. *IEEE Trans. Power Electron.* **2006**, *53*, 1002–1016. [\[CrossRef\]](#)
- Raju, E.S.N.P.; Trapti, J. Hybrid AC/DC micro grid: An overview. In Proceedings of the Fifth International Conference on Power and Energy Systems, Kathmandu, Nepal, 28–30 October 2013.
- Liu, X.; Wang, P.; Loh, P.C. A hybrid AC/DC microgrid and its coordination control. *IEEE Trans. Smart Grid* **2011**, *2*, 278–286.
- Unamuno, E.; Barrena, J.A. Hybrid AC/DC microgrids-part I: Review and classification of topologies. *Renew. Sustain. Energy Rev.* **2015**, *52*, 1251–1259. [\[CrossRef\]](#)
- Loh, P.C.; Ding, L.; Yi, K.C.; Frede, B. Autonomous operation of hybrid microgrid with AC and DC sub-grids. *IEEE Trans. Power Electr.* **2013**, *28*, 2214–2223. [\[CrossRef\]](#)
- Singh, A.; Surjan, B.S. Microgrid: A review. *Int. J. Res. Eng. Technol.* **2014**, *3*, 185–198.
- Hatziargyriou, N. *Microgrids: Architectures and Control*; IEEE Press: Baltimore, MD, USA, 2014.
- Lasseter, R.H.; Paigi, P. Microgrid: A conceptual solution. In Proceedings of the IEEE Power Electronics Specialists Conference, Aachen, Germany, 20–25 June 2004.
- Garcés, S.I.; Montoya, D.G.; Ramos, C.A. Sliding-mode control of a charger/discharger DC/DC converter for DC-bus regulation in renewable power systems. *Energies* **2016**, *9*, 245. [\[CrossRef\]](#)
- Guerrero, J.M.; Vasquez, J.C.; Matas, J.; De Vicuña, L.G.; Castilla, M. Hierarchical control of droop-controlled AC and DC microgrids—A general approach toward standardization. *IEEE Trans. Ind. Electron.* **2011**, *58*, 158–172. [\[CrossRef\]](#)

15. Rocabert, J.; Luna, A.; Blaabjerg, F.; Rodriguez, P. Control of power converters in AC microgrids. *IEEE Trans. Power Electron.* **2012**, *27*, 4734–4749. [[CrossRef](#)]
16. Katiraei, F.; Iravani, M.R.R. Power management strategies for a microgrid with multiple distributed generation units. *IEEE Trans. Power Syst.* **2006**, *21*, 1821–1831. [[CrossRef](#)]
17. Majumder, R.; Ghosh, A.; Ledwich, G.; Zare, F. Power management and power flow control with back-to-back converters in a utility connected microgrid. *IEEE Trans. Power Syst.* **2010**, *25*, 821–834. [[CrossRef](#)]
18. Akhuleh, S.P.; Mokhtari, H.; Blaabjerg, F. Hierarchical Power Sharing Control in DC Microgrids. In *Microgrid: Advanced Control Methods and Renewable Energy System Integration*; Butterworth-Heinemann: Oxford, UK, 2017; pp. 63–100.
19. Chaudhuri, N.R.; Chaudhuri, B.; Mujumder, R.; Yazdani, A. *Multi-Terminal Direct-Current Grids: Modeling, Analysis and Control*; John Wiley & Sons: Hoboken, NJ, USA, 2014.
20. Nasirian, V.; Davoudi, A.; Lewis, F.L.; Guerrero, J.M. Distributed adaptive droop control for DC distribution systems. *IEEE Trans. Energy Convers.* **2014**, *29*, 944–956. [[CrossRef](#)]
21. Morstyn, T.; Hredzak, B.; Demetriades, G.D.; Agelidis, V.G. Unified distributed control for DC microgrid operating modes. *IEEE Trans. Power Syst.* **2016**, *31*, 802–812. [[CrossRef](#)]
22. Morstyn, T.; Hredzak, B.; Agelidis, V.G. Cooperative multi-agent control of heterogeneous storage devices distributed in a DC microgrid. *IEEE Trans. Power Syst.* **2016**, *31*, 2974–2986. [[CrossRef](#)]
23. Peyghami, S.; Mokhtari, H.; Blaabjerg, F. Autonomous operation of a hybrid AC/DC microgrid with multiple interlinking converters. *IEEE Trans. Smart Grid* **2017**, *PP*. [[CrossRef](#)]
24. Ma, T.; Cintuglu, M.H.; Mohammed, O.A. Control of hybrid AC/DC microgrid involving energy storage and pulsed loads. *IEEE Trans. Smart Grid* **2014**, *53*, 567–575. [[CrossRef](#)]
25. Baghaee, H.R.; Mirsalim, M.; Gharehpetian, G.B.; Talebi, H.A. A decentralized robust mixed H_2/H_∞ voltage control scheme to improve small/large-signal stability and FRT capability of islanded multi-DER microgrid considering load disturbances. *IEEE Syst. J.* **2017**, *99*, 1–12.
26. Xu, Y. Robust finite-time control for autonomous operation of an inverter-based microgrid. *IEEE Trans. Ind. Inform.* **2017**, *13*, 2717–2725. [[CrossRef](#)]
27. Yu, X.; Starke, M.R.; Tolbert, L.M.; Ozpineci, B. Fuel cell power conditioning for electric power applications: A summary. *IET Electr. Power Appl.* **2007**, *1*, 643–656. [[CrossRef](#)]
28. Seyedmahmoudian, M.; Mekhilef, S.; Rahmani, R.; Yusof, R.; Taslimi, E. Analytical modeling of partially shaded photovoltaic systems. *Energies* **2013**, *6*, 128–144. [[CrossRef](#)]
29. Jiao, J. Sliding mode control for stabilizing of boost converter in a solid oxide fuel cell. *Cybern. Inf. Technol.* **2013**, *13*, 139–147. [[CrossRef](#)]
30. Ayad, M.Y.; Becherif, M.; Djerdir, A. Sliding mode control for energy management of DC hybrid power sources using fuel cell, batteries and supercapacitors. In Proceedings of the IEEE International Conference on Clean Electrical Power, Capri, Italy, 21–23 May 2007.
31. Kishinevsky, Y.; Zelingher, S. Coming clean with fuel cells. *IEEE Power Energy Mag.* **2003**, *99*, 20–25. [[CrossRef](#)]
32. Larminie, J.; Dicks, A. *Fuel Cell Systems Explained*; Wiley: Chichester, UK, 2003.
33. Moldrik, P.; Chvialek, R. PEM fuel cells—The basic characteristics. In Proceedings of the IEEE International Conference on Environment and Electrical Engineering, Rome, Italy, 8–11 May 2011.
34. Benziger, J.B.; Sattereld, M.B.; Hogarth, W.H.; Nehlsen, J.P.; Kevrekidis, I.G. The power performance curve for engineering analysis of fuel cells. *J. Power Sources* **2006**, *155*, 272–285. [[CrossRef](#)]
35. Hoogers, G. *Fuel Cell Technology Handbook*; CRC Press: Boca Raton, FL, USA, 2003.
36. Saadi, R.; Bahri, M.; Ayad, M.Y.; Becherif, M.; Kraa, O.; Aboubou, A. Implementation and dual loop control of two phases interleaved boost converter for fuel cell applications. In Proceedings of the IEEE International Symposium on Environmental Friendly Energies and Applications (EFEA), Paris, France, 19–21 November 2014.
37. Kabalo, M.; Paire, D.; Blunier, B.; Bouquain, D.; Simões, M.G.; Miraoui, A. Experimental validation of high-voltage-ratio low-input-current-ripple converters for hybrid fuel cell supercapacitor systems. *IEEE Trans. Veh. Technol.* **2012**, *61*, 3430–3440. [[CrossRef](#)]
38. Kabalo, M.; Paire, D.; Blunier, B.; Bouquain, D.; Simões, M.G.; Miraoui, A. Experimental evaluation of four-phase floating interleaved boost converter design and control for fuel cell applications. *IET Power Electron.* **2013**, *6*, 215–226. [[CrossRef](#)]

39. Sabzegar, R.; Moallem, M. Modeling and control of a boost converter for irregular input sources. *IET Power Electron.* **2012**, *5*, 702–709. [[CrossRef](#)]
40. Bacha, S.; Munteanu, I.; Bratcu, A.I. *Power Electronic Converters Modeling and Control*; Springer: London, UK, 2014.
41. Krein, P.T.; Bentsman, J.; Bass, R.M.; Lesieutre, B. On the use of averaging for analysis of power electronic system. *IEEE Trans. Power Electron.* **1990**, *5*, 182–190. [[CrossRef](#)]
42. Chen, J.; Erickson, R.; Maksimovic, D. Averaged switch modeling of boundary conduction mode DC-to-DC converters. In Proceedings of the IEEE Industrial Electronics Society, Denver, CO, USA, 29 November–2 December 2001.
43. Hirschorn, R.M. Generalized sliding-mode control for multi-input nonlinear systems. *IEEE Trans. Autom. Control* **2006**, *51*, 1410–1422. [[CrossRef](#)]
44. Slotine, J.J.; Li, W. *Applied Nonlinear Control*; Prentice Hall: Englewood Cliffs, NJ, USA, 1991.
45. Zhong, Q.; Weiss, G. Synchroverters: Inverters that mimic synchronous generators. *IEEE Trans. Ind. Electron.* **2011**, *58*, 1259–1267. [[CrossRef](#)]
46. Zhong, Q.; Weiss, G. Static synchronous generators for distributed generation and renewable energy. In Proceedings of the 2009 IEEE/PES Power Systems Conference and Exposition, Seattle, WA, USA, 15–18 March 2009.
47. Beck, H.; Hesse, R. Virtual synchronous machine. In Proceedings of the 2007 9th International Conference on Electrical Power Quality and Utilisation, Barcelona, Spain, 9–11 October 2007.



© 2017 by the authors. Licensee MDPI, Basel, Switzerland. This article is an open access article distributed under the terms and conditions of the Creative Commons Attribution (CC BY) license (<http://creativecommons.org/licenses/by/4.0/>).